International Journal of Recent Advances in Multidisciplinary Topics
Volume 2, Issue 11, November 2021
https://www.ijramt.com | ISSN (Online): 2582-7839

Aerodynamics of Hovering Hummingbird

P. N. Shahanas[1*], M. Yoga Prakash[2], S. Suvitha[3], R. S. Aswin[4], K. Manoj Kumar[5]
[1,2,3,4]*Student, Department of Aeronautical, Hindusthan College of Engineering and Technology, Coimbatore, India*
[5]*Assistant Professor, Department of Aeronautical, Hindusthan College of Engineering and Technology, Coimbatore, India*

***Abstract*: While studying about aerodynamics or aeronautical engineering first thing which comes to our mind is how to fly like birds or insects. As the birds are amazing example of flying object, insects are too that much interesting. They got some remarkable manoeuvring skill that hovering. In birds, only humming bird have this ability to hover. The capability of hummingbird to hover gives us a curiosity to study about the fundamentals of the hover. We explained the whole analysis very beautifully and in a fascinating manner.As in this era of advance aerodynamics, the concept of hovering hummingbird and its manoeuvring help us to develop an efficient aircraft. This report enhances our understanding in the field of aerodynamics. Briefing our ted talk, we as a team did something really noteworthy and want other to have look on this report. We read almost more than 30 article and research paper to make our report that worthy of it.**

***Keywords*: Aerodynamic, Downstroke, Hummingbird, Lift, Speed, Wing.**

1. Introduction

Many studies have been done to characterize the kinematics, physiology and aerodynamics of the hummingbird wing, and they were summarized in the work of to balske et al. In general, Humming birds use similar aerodynamics to those of insects, e.g., presence of a leading-edge vortex over the wing surface, for lift production. However, differences between hummingbird and insect aerodynamics are conceivable as the anatomy and physiology of the hummingbird wing are distinct from those of the insect wing2. For example, recent evidence shows that hummingbirds can achieve the inversion of the angle of attack through active wing rotation at the wrist 2. This actuation mechanism is different from that of insects whose wing inversion can be realized through combined muscle activation at the wing root and the passive deformation of the wing surface1.The implication of this difference on the lift and power efficiency of hummingbirds is still unclear. The aerodynamic ability to stay airborne while hovering must be preserved throughout the entire annual cycle, including during the energy-demanding period of feather moult, in which wing surface is reduced. Studies of free-flying hummingbirds have found the lift production to be asymmetric between the stroke halves, where the power stroke, 2 denoted herein as the down stroke, produces up to 75% of the weight support, contrary to insects where wing support is symmetric 2 The authors reported that the intensity of this vorticity is highly variable and corresponded to changes between 02. In hummingbirds, the mass ratio between the supracoracoideus and pectoralis, the flight muscles corresponding to the upstroke and down stroke, is among the highest found in nature. They were able to measure the flow in the two dimensional planes that are perpendicular to the wing axis during the entire stroke cycle. 1 times of that during the upstroke. For example, the wing velocity and the angle of attack during the downstroke are greater than those during the upstroke. Other variables they suggested include longer wing span and formation of a positive camber during the downstroke. Despite these previous efforts, there exists no direct study on the detailed force characteristics and the three-dimensional flow pattern of the hummingbird wing in hovering flight.

1) Wing design

Based on a three-dimensional three-dimensional laser examination, a perfect male wing of C. anna, and a 3. 5: 1, alternately the limited model wing is built using stereolithography. Previous studies have found that the hummingbird's wings are strong, especially in time stroke. In addition, electron scanning microscope measurements of the C. anna wing are shown a physical connection between neighboring barbs, justifying the use of a rigid and non-porous material for the wing model in our experimental scheme presented below. It is also assumed that wing deformation is minimal and does not play a significant role during the down stroke due to special feather arrangement, as opposed to during upstroke and wing reversal. Therefore, only the down stroke is analyzed herein. Regarding wing reversal, there is evidence that it contributes additional circulation generated as the wing rotational velocity decays. However, it is believed that higher fidelity results are required in order to adequately quantify this aspect and consequently it will be the subject of a future study.

2. Experimental Method

To investigate the flow over the Anna's hummingbird wing, time-accurate measurements of the aerodynamic loads acting on the wing, along with flow field measurements using phase-

*Corresponding author: shahanasshanuz143@gmail.com

locked particle image velocimetry , were conducted. The study was carried out using a pair of wings suspended in a tank filled with a working fluid that varied between the two sets of experimental set-ups to meet the aerodynamic similarity constraints and their inherent limitations. A controller unit (Technosoft IPOS3604- VX-CAN, Neuch tel, Switzerland) controlled a servomotor (3257CR32A, Faulhaber, Sch naich, Germany) which rotated the wing pair around a vertical axis. Each wing followed stages of initial acceleration, steady rotation and deceleration to model the downstroke of a flapping wing3.The motion command was subjected to the kinematical constraint of approaching mid-downstroke, where = 90, at the middle of each wing cycle (denotes the wing's angular position, figure 1d)3 .These simplifications allowed us to coherently analyse the basic flow mechanisms that developed over the wing at one distinct Reynolds number, avoiding second order effects3. In this study, Re=10000 and is defined as = 90 based on the wing tip velocity at middownstroke, U90tip =, and the mean chord,. R is one wing span, is the dimensionless distance between the wing's root and the centre of rotation, is the angular velocity at mid-downstroke and is the kinematic viscosity of the working fluid.At the end of each wing stroke, a pause of approximately 30 s took place to establish an essentially quiescent flow at the beginning of each wing stroke. The time-averaged lift coefficient required to support the bird's body weight (divided by two, in order to refer to one wing) is where mb is Anna's hummingbird's body mass during the moulting period, g is the gravitational acceleration, $\boldsymbol{\rho a}$ is the air density at sea level and $\boldsymbol{fb}$ is the wingbeat frequency, defined as 40 Hz. $\boldsymbol{Sb}$ and $\boldsymbol{R2}$? are the complete wing area and radius of the second moment of area, respectively3.

$$\overline{\zeta'^2} = \left(\frac{1}{n}\right)\sum_{i=1}^{n}[(\zeta_i - \zeta)U_{\parallel}/U_{tip}^{90^\circ}]^2,$$

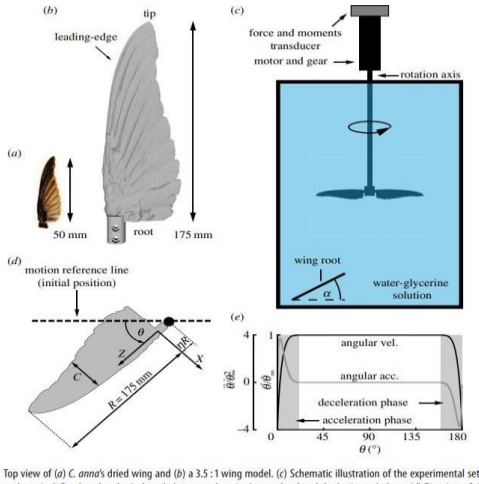

Figure 1. Top view of (*a*) *C. anna*'s dried wing and (*b*) a 3.5 : 1 wing model. (*c*) Schematic illustration of the experimental set-up. The angle of attack, α, is defined as the physical angle between the wing's root chord and the horizontal plane. (*d*) Top view of the wing, depicting the coordinate system. (*e*) The wing motion kinematics, where $\dot{\theta}$ and $\ddot{\theta}$ are the instantaneous angular velocity and acceleration, respectively. $\dot{\theta}_{\infty}$ is the angular velocity at mid-downstroke ($\theta = 90^\circ$).

Fig. 1. Top view

3. Flow Field Measurement

Flow field measurements were obtained at α = 30° using image velocimetry of phase-locked particles (PIV). Our experimental setup included PIV system (Dantec Dynamics A / S, Skovlunde, Denmark) covering dual-cavity 30 ml Nd: YLF laser with a repetition rate of up to 10 Hz, 4M pixel 12-bit CCD camera adjustment (Flow Sense EO) once a systematic time unit. Two tests schemes were used. The first rated in-part of the plane speed at different angular positions near downstroke (θ) over three span channels, i.e., z = r / R = 0.25, 0.5 and 0.75, wherer is the dimensional distance of the span channel from wing of the wing. The second measured close-wake speed field at channels representing weight loss (see paragraph 2). Unstable speed field of magnitude is defined as where Ui is a flow field found in ith average ($1 \leq i \leq n$). U, V and W are speed sections in X, Y and Z, respectively (see Figure 1). Tangential velocity in each space the channel says $U\parallel (z) = \theta \cdot R (z + \eta)$, where η is flawless distance between the root of the wing and rotation center (referred to R; see fig. 1d at [30]). Dimensionless speed field on the wing the reference framework is defined as U = {U - U‖, V, W} / U‖ = {u, v, w}.Near-speed field-points refer to the tip of the wing speed, ∗ = u / Utip, where Utip = θ˙R (1 + η). Because statistical analysis, speed fluctuations are present defined using a standard definition wing speed during stroke,show a different correlation between torque coefficient, CQ, and angular velocity profile (Figure 3b).Timely development of aerodynamic timing loads are limited in time for proper operation to measure all aerodynamic features of downstroke (as shown in equations). Time- central aerodynamic coefficient, ¯ or ¯, (shown in Figure 3c),showing similar styles as measured in previous studies dried with hummingbird wing features and insect wings with the same aspect ratio (table 1). To be clear, the error bars represents a standard five-fold deviation times, indicating a high repetition of results.While the elevation rises monotonically to 5 ° ≤ α ≤ 20 °, as raised from the exact time to raise the coefficients (Figure 3a), I the medium-term torque coefficient, ¯, increased parabolic at an angle of attack, giving a maximum {¯/¯} of about 6 at α = 5 °(image 3d).Due to the significant reduction in lifting capacity in the area the early stages of the moult cycle, in which the wing area is the smallest, we introduce waking rates near a the missing wing P1-4 in figure 4. These ratings introduce tip development vortex for all downstroke and active disk space created over rotation or batting wings and is characterized by a negative shape speed values related to lift. To enable acompared to the full wing, the active disc space provided relative to wing disk (Sd = π [(R + Rη) 2 - (Rη) 2]).Except for the vortex of a well-established basic tip formed at the tip of the wing in the early stages of downstroke, small, clockwise, second vortex appeared in the middle of the gap, working effectively as a tip (θ = 22.5◦, figure 4a, b). Active disc the area is closed between two vortices (primary and second) over the middle part of the wing, covering 65% of the wing disc area(Figure4a). By mid-stroke, tip vortex is fully separated as well the dynamic flow continues from one point to the root (number 4c, d). Active disk space moved up and finally covers 42% of the wing disc area. Overall, the non-league area created a 16% reduction in effective disc area compared a complete wing throughout the downstroke (e.g. 5). Reduction of effective disk space resulted in a the quality level of lift damage as seen

with aerodynamic loads obtained over P1-4 wing (figure 3c).To better understand the effect of moult on the main flow characteristics, comparisons are made between flow fields are measured in the middle of the span and in the middle of the stroke (z= 0.5, θ = 90◦) over complete wing, P1-4 and P10 (Figure 5). Flow field over full wing shows two different flow characteristics: accelerated flow above the edge covering about 0.3c (where c area chord length) and large separated flow the area that forms behind the wing that appears to be large amounts of flow fluctuations (Fig. 5a, d). As shown complete wing, these flow characteristics developed until mid-stroke and remained the same in size and power throughout the rest stroke. Above the wing of P1-4 (Fig. 5b), I the accelerated area above the front edge is comparable in size and power to the full wing. I the gap created by the missing feathers is delayed flow separation, which continued to improve until the end of the downstroke. They are not drunk fragmentation may have been created to exist of the vortex of the second tip (Fig. 4), introduces improved mixing near the gap. This causes a high pressure applied to a boundary layer, which causes it to stick to the wing moves forward near the downstroke .Consequences of a deficit of the top 10 aircraft can be seen in Figure 5c, f. At this stage, it is great accelerated flow circuit improved over lead-edge. In addition, low flow rate fluctuations was measured. This flow fluctuation was enhanced by near the wing area and as a result associated with an advanced boundary layer with a song. Active active growth radius, however, is only delayed in the separation of the flow over span, it comes out in full z = 0.75, the same as z z value of the whole unit.We have explored the importance of leadership once and for all the tip of the wing tip by measuring the flow near the wake wing field P89 (Figure 6). In this wing configuration, the wing is 11% deficient in its area location, and the gap is found mostly over the distal part of the wing. We found a gap in the wing causing the tip vortex to break even at the beginning downstroke stages (Figure 6a, b), in contrast to a well-constructed tip vortex that was over complete and P1-4 wings (Fig. 4a, b). Like result, an effective, easy disk space between tip and root vortices, covered 0.63Sd, 19% reduction compared to the full unit in this stage. Continued down stroke (Fig. 6c, d), I active disk space includes 0.2Sd area, 40% decrease compared to that of the whole unit in this is the downstroke phase. Like a working disk the area is associated with the production of lift, large the decrease in its size shows greatness aerodynamic damage to this wing suspension. Vertical speed distribution near length of P89 and full wings continuously indicates a reduction in lift if integrity wing tip disabled (Fig. 6a, c). Although the same values of negative vertical speed were measured within an effective disk space, without it, weak negative speed and direct precision measured in P89 unit compared to full wing, which raises an additional drop in lifting wing production. We checked I the importance of precision and the integrity of the wing tip in measuring the flow field adjacent to the P89 wing lift (Figure 6). In this wing formation, the wing is is 11% short of its territory, and the gap is huge is located on the far side of the wing. We got it that a gap in the wing caused the tip vortex to break down even in the early stages of downstroke (Fig. 6a, b), in contrast to the vortex of a well-formed tip which was on top of the whole and P1-4 (Fig. 4a, b) wings. As a result, an effective disclocation, extension between tip and root vortices, covere 0.63Sd, a 19% decrease compared to a complete unit in this category.

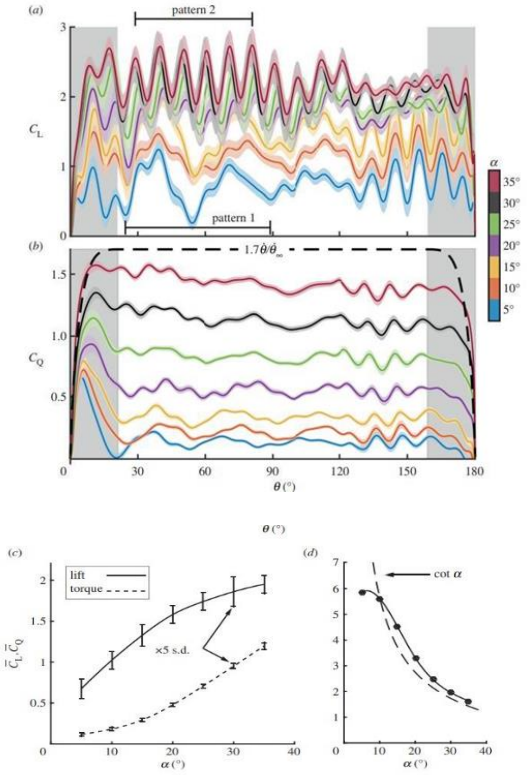

Figure 3. Time-accurate aerodynamic coefficients along the downstroke at all tested angles of attack: (*a*) lift (*b*) torque due to drag. Solid lines denote ensemble-averaged values; shaded regions represent the standard deviation (s.d.) value at each angular position. The dashed line in (*b*) represents the wing angular velocity profile along the downstroke. (*c*) Time-averaged aerodynamic coefficients at different angles of attack. Error bars represent the time-averaged standard deviation of measurements, magnified five times, for clarity. (*d*) Lift-to-torque ratio, compared to Polhamus leading-edge vortex geometric model of cot α [43], denoted by a dashed line.

Fig. 2. Time accurate aerodynamics

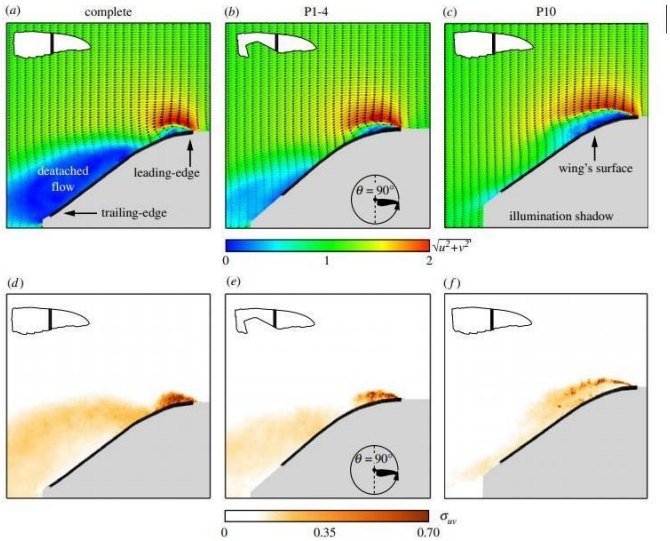

Figure 5. Flow fields (*a–c*) at $\alpha = 30°$ and their corresponding flow fluctuation values (*d–f*) at mid-stroke over the medial span station ($\theta = 90°$ and $z = 0.5$) at different stages of moult: (*a,d*) complete wing; (*b,e*) P1-4 wing; (*c,f*) P10 wing. The first row's colour scheme describes the in-plane velocity magnitude, $\sqrt{u^2 + v^2}$. The solid black line depicts the wing position and the shaded grey areas represent the illumination shadow region behind it.

Fig. 3. Flow fields

Further down the stroke(Fig. 6c, d), effective disk space covers space of 0.2Sd, a 40% decrease compared to that of a

complete wing in this phase of down stroke. As I the active disc area is associated with lifting production, a significant reduction in its size indicates a greater aerodynamic damage to this wing suspension. Vertical speed distribution near length of P89 and full wings continuously indicates a reduction in lift if integrity wing tip disabled (Fig. 6a, c). Although the same values of negative vertical speed were measured within an effective disk space, without it, weak negative speed and direct precision measured in P89 unit compared to full wing, which raises an additional drop in lifting wing production.

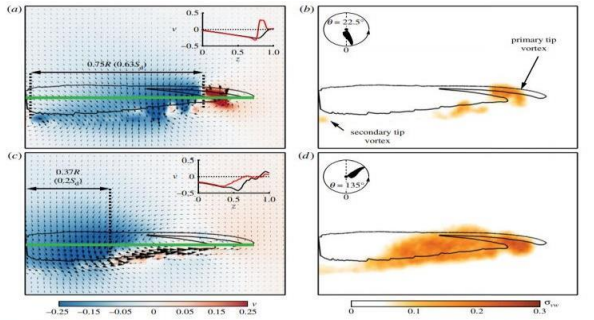

Figure 6. Near-wake measurements over a P89 wing configuration at $\alpha = 30°$; $(a,b)\ \theta = 22.5°$; $(c,d)\ \theta = 135°$. See figure 4 for panel description. In the insets, vertical velocity along the span (green line) is compared between the complete [30] (black line) and P89 (red line) wings.

Fig. 4. Near wake measurements

4. Discussion

Hovering is a necessary type of aircraft as a weight support is the sole function of the aircraft muscles' skills. To evaluate the effects of oscillating aerodynamic loads and wing fluctuations Performance, decrease in time scale aerodynamic coefficients are used for measurement all features of aerodynamic wingbeat in between to walk. Coefficient of medium term lift required to support the body weight of the bird is where mb = 4.6 0. 22 g is Anna's body weight, g is her gravitational acceleration, a density of sea air rate and fb wing beat frequency. Sb and R2b the location of the bird's wing and the second radius local moment, respectively. Flow field Estimates show that 66% to 75% of weight support is provided by the downstroke movement of C Anna's wing.

So, all natural wingbeat the medium-term elevator can be indirectly measured from production of downstroke lift, rated in the current setting. With equal downstroke too upstroke length. For biological examination conditions in which Anna hummingbirds travel, an aerodynamic lift is needed to support the bird weight; therefore, =. According to the equation, downstroke wing movement is required to provide lift coefficient of = to provide sufficient height in the middle of every wingbeat. Under the terms described above, downstroke average lifted time the coefficient should reach a maximum value =1.44 0. An element of power, representing Annathe efficiency of the hummingbird aircraft, is described as as opposed to the aerodynamic forces required for support unit of weight, = where M is the weight to be raised and = /. Links between aerodynamic lift and drag allows us to think the same h in order to balance contribution of downstroke to general aerodynamic torque and power. Muscles around me 'aerodynamic power output during downstroke, P, calculated (multiplied by 2 to refer to the wing pair) using precise aerodynamic torque on time pull: = R3b is the hummingbird wing of Anna hummingbird of the third minute of the place. Tea & Millard measures the maximum size of a wingbeat for a certain strength different species of hummingbird by their experiments high loading capacity. Valid offer compared to our results, Chai & Millard's maximal power values are translated to reflect the ratio reduce certain power using equation. I the red shaded area in Figure 9b corresponds to the time- high downstroke loading capacity, where the lower limit corresponds to S.rufus. As expected, a very high amount of energy is in the middle of speeding up the phase, when the muscles need to win the inertia of the wings. Despite the onset of high energy. It is believed to be Anna's hummingbird it works well in a safe environment everywhere of downstroke, as suggested by Chai & Millard, which allows for the conservation of large amounts of energy in the air directing (e.g., high-speed dating aircraft). Wing performance We divide the two basic elements into balance energy requirements while moving upwards by moulting wing, bird body weight and downstroke contribution to the total increase produced by a wingbeat, h Regarding weight loss, Chai reported that ruby-throated hummingbirds deplete their body weight by about 25% during moult in related stages with the loss of wing area corresponding to P1-4 as well SP6 wings in our study. Epting reported 10% weight loss of a black-chinned person a hummingbird after breaking the 10th remote tip first flight feathers and different body levels mass reduction in different stages of moult on an Each Allen5 buzzer. Moreover, it will still be seen if the birds lose their body weight during moult whether their moult stage, or if they adjust their body weight by corresponding area over the wing with various categories of moult sequence as suggested by Epting5 If I Lastly it is true, aerodynamic strength is required by weight support can vary greatly during the whole growing season due to hummingbird moult the cycle involves reducing the area of the wing to be different width. In addition, the hummingbird's body weight varies very all day long, and the flexibility.

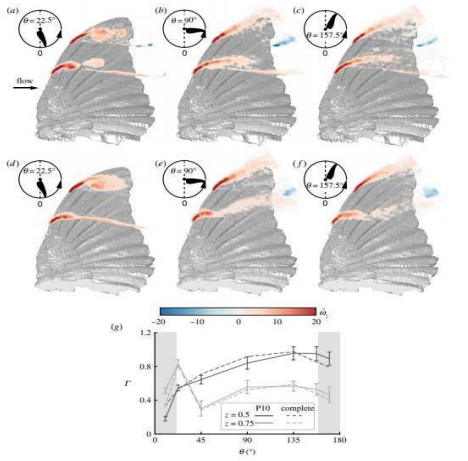

Spanwise vorticity fields at $\alpha = 30°$ over the P10 wing at $(a)\ \theta = 22.5°$; $(b)\ \theta = 90°$; $(c)\ \theta = 157.5°$, and over the complete wing at $(d)\ \theta = 22.5°$; $(e)\ \theta = 90°$; $(f)\ \theta = 157.5°$. The vorticity fields are presented at the measured span stations $z = 0.5$ and $z = 0.75$. (g) Net circulation at the corresponding span stations over both wings. Grey areas are the acceleration and deceleration phases of the wing motion. Error bars represent the standard deviation of the circulation over the P10 wing. For the standard deviation of the complete wing and wing kinematics, see [30].

Fig. 4. Span wise vorticity

5. Conclusion

In the current offer, we focus on configuration of the base wing while setting the foundations of our analysis strategies will be used to deal with flow processes as well aerodynamic features of several wings geometries showing several categories wing moult cycle. Flow field over the wing revealed the unstable concentration of spanwise vorticity built and demolished near on the front edge. In this bubble, the flow separates again creates an environment with low pressure, similar to that emerged within the vortex of the leading edge. I the difference between the two is that in the beginning, Vortex depletion also appears, introducing more time measurements in this flow field. At the end of a stroke, these the focus of vorticity is discarded down-wash and a new moving bubble is being created. The nature of leadership instability- the hem bubble is exposed to an accurate load of time measurements and well matched details flow analysis of the flow field. In addition, the presented method allows for more detailed and precise information investigation of the hummingbird's wing function; this method can be used to further investigate further features of the most complex aerodynamics hummingbirds and parallel flow patterns such as a loss of wing and a rise in disability wings. Simulation captures lift and power features on the side cycle and details of flow field. Our result confirms and provides directness lifting asymmetry data that previously existed suggested based on the rating of around the wing. Moreover, we critically analyze the sources of the proposal asymmetry and pointed out ways that lead

References

[1] Hummingbird flight Douglas Warrick et.al
[2] Haoxiang Luo Three-dimensional flow and lift characteristics of a hovering ruby-throated hummingbird
[3] Hovering hummingbird wing aerodynamics during the annual cycle. I. Complete wing. Yonathan Achache et.al
[4] Epting RJ et.al. Functional dependence of the power for hovering on wing disc loading in humming birds. Physiol. Zool. 53, pp. 347–357. 5.
[5] Barta Z et.al. Optimal moult strategies in migratory birds. Phil. Trans. R. Soc. B 363, pp. 211–229.